Published by Nigerian Society of Physical Sciences. Hosted by FLAYOO Publishing House LTD

Recent Advances in Natural Sciences

Journal Homepage: https://flayoophl.com/journals/index.php/rans

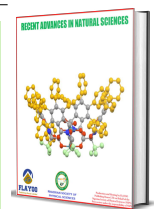

Green synthesis of Cu, Fe, and Cu/Fe nanomaterials using *Khaya senegalensis* and investigation of their photocatalytic reduction of 4-nitrophenol and antibacterial properties

J. I. Kuv[a], J. A. Attah[a], I. Hassan[a], O. G. Uyi[b], A. D. Terna[c], M. E. Binin[a], A. H. Labulo[a,*], A. A. Idzi[a], M. Isah[d], S. M. Idris[b], M. A. Alabi[a], K. A. Ojedoja[a], A. Y. Danas[a], F. O. Ogungbemiro[e], F. H. Omotehinwa[f], J. O. Anebi[e]

[a]*Department of Chemistry, Federal University of Lafia, Nigeria*
[b]*Department of Microbiology, Federal University of Lafia, Nigeria*
[c]*Department of Chemistry, Federal University of Technology Owerri, Nigeria*
[d]*Department of Science Laboratory Technology, Federal University of Lafia, Nigeria*
[e]*CBIOS-Research Center for Biosciences & Health Technologies, Universidade Lusófona de Humanidades e Tecnologias, Campo Grande 376, Lisboa, Portugal*
[f]*Department of Chemistry, Federal University of Health Sciences, Otukpo, Nigeria*

ARTICLE INFO

Article history:
Received: 27 October 2025
Received in revised form: 08 December 2025
Accepted: 11 December 2025
Available online: 31 December 2025

Keywords: Green synthesis, Catalytic properties, Antibacterial activity, Bimetallic nanoparticles, *Khaya senegalensis*

DOI:10.61298/rans.2025.3.2.236

ABSTRACT

The persistent environmental and health threats posed by nitroaromatic pollutants—particularly 4-nitrophenol (4-NP)—and the rise of multidrug-resistant bacterial pathogens demand sustainable, efficient, and eco-friendly remediation strategies. To address these challenges, this study developed monometallic (CuO and Fe_2O_3) and bimetallic (CuO/Fe_2O_3) nanoparticles via a green, one-pot synthesis using *Khaya senegalensis* leaf extract, leveraging its rich phytochemical content as natural reducing and capping agents. The synthesized nanoparticles were characterized using UV–Vis spectroscopy, XRD, FTIR, and HAADF STEM, confirming the formation of spherical, monodispersed particles (20 nm to 50 nm) with distinct surface plasmon resonance peaks at 224 nm (CuO), 290 nm (Fe_2O_3), and a redshifted peak at 295 nm (CuO/Fe_2O_3). The XRD analysis revealed the crystallite sizes of CuO, Fe_2O_3 and CuO/Fe_2O_3 NPs to be 26 nm, 22 nm and 28 nm, respectively. Bimetallic CuO/Fe_2O_3 nanocomposite demonstrated exceptional photocatalytic efficiency, achieving complete reduction of 4-NP to 4-aminophenol in just 2 min, over 50% faster than monometallic counterparts. Furthermore, it exhibited potent antibacterial activity, with minimum inhibitory concentrations (MIC) of 8 µg/mL against *Escherichia coli* and *Bacillus subtilis*, and 40 µg mL^{-1} against *Pseudomonas aeruginosa*, alongside minimum bactericidal concentrations (MBC) of 16 µg/mL and 80 µg/mL, respectively. These results underscore the multifunctional potential of *K. senegalensis*-derived CuO/Fe_2O_3 nanocomposites as green, high-performance agents for simultaneous environmental detoxification and antimicrobial applications. We recommend their further development for scalable water treatment and as alternatives to conventional antibiotics, particularly against resilient Gram-negative pathogens.

*Corresponding author Tel. No.: +234-806-2295-936
e-mail: ayomide.labulo@science.fulafia.edu.ng (A. H. Labulo)

1. INTRODUCTION

The unique characteristics of nanoparticles in the physical, biological, and chemical realms allow for a broad and versatile application of nanoparticles in many different areas. They have advanced medicine, biotechnology, and the environmental sciences, as well as the interdisciplinary fields of catalysis and energy research [1]. Iron (Fe) and copper (Cu) in their hybrid and copper-iron (Cu/Fe) formats are also used. The remarkable optical, electrical, and magnetic, as well as the catalytic properties of nanoparticles have attracted considerable attention within the scientific community [2, 3]. Their remarkable properties have also enabled their application in the purification of water, magnetic resonance imaging, drug delivery, biosensing, antibacterial therapy, and other nanoparticle-associated therapies [4, 5].

That being said, traditional methods for nanoparticle fabrication such as chemical reduction, sol-gel synthesis, and co-precipitation, have certain limitations [5, 6]. These limitations stem from complex procedures, excessive energy use, the potential for bodily harm, and the requirement for expensive and specialized tools [6, 7]. These methodological shortcomings negatively impact the environment and pose risks to human health, thereby reducing the potential for scalability and compromising the yield of stable nanoparticles. Hence, a need for a simpler, more economical, and environmentally benign approach to nanoparticle synthesis.

One of these techniques is the use of plant extracts in the synthesis of metal nanoparticles [7, 8]. Plant extracts contain phytochemicals such as phenols, flavonoids, terpenoids, alkaloids and others. During synthesis, metal ions are reduced and barriers preventing oxidation and clumping are formed [5, 9]. This plant-mediated route is considered a green synthesis approach because the *K. senegalensis* extract functions simultaneously as a natural reducing and capping agent, avoiding toxic reagents, minimizing hazardous waste, and enabling nanoparticle formation under mild, energy-efficient conditions consistent with green chemistry principles [10].

The leaf extract of *Khaya senegalensis* is well known for its use in the treatment of microbiological infections, diabetes, pain, inflammation, fever, and malaria. This medicinal plant is indigenous to Africa and Asia. *K. senegalensis* has numerous bioactive compounds that are capable of serving as reducing and capping agents and have antibacterial, anti-inflammatory, and antioxidant qualities, hence the choice of the plant extract for the current study [11, 12]. Despite exploration of the therapeutic potency of the plant extract, there remain unexplored aspects within the literature regarding the synthesis and the characterization of CuO, Fe_2O_3, and CuO/Fe_2O_3 nanoparticles utilizing *K. senegalensis* extract, as well as the evaluation of their antibacterial and catalytic properties.

Nitrophenols, particularly 4-nitrophenol (4-NP), are primarily introduced into the environment through industrial effluents from pesticide, dye, pharmaceutical, and explosive manufacturing processes [13, 14]. Although nitrophenol serves as an important chemical building block, it is also an extremely destructive soil and water pollutant due to its high water solubility and persistence. It poses significant danger to all forms of life [13]. Compared to conventional physicochemical remediation approaches such as activated-carbon adsorption and chemical oxidation, biological remediation techniques have been reported to offer higher environmental compatibility, greater selectivity, and reduced secondary pollution [15]. Nonetheless, biological methods suffer from poorly defined suitable microbial agents and slow reaction velocities [15]. Of all nitrophenols, 4-nitrophenol is the most toxic. Its electron-withdrawing nitro group renders it resistant to hydrolysis, biological degradation, and chemical oxidation. More innovative approaches will be necessary to overcome this recalcitrance [13, 14].

4-Nitrophenol was selected as a model pollutant due to its widespread presence in industrial wastewater, high toxicity, environmental persistence, and ease of detection via UV-Vis spectroscopy (notably its intense yellow color and characteristic absorbance at ~400 nm under alkaline conditions) [13]. The conversion of 4-nitrophenol to 4-aminophenol is driven by catalytic reduction (e.g., using $NaBH_4$ and a catalyst), which transforms the nitro group ($–NO_2$) into an amino group ($–NH_2$) [15]. This reduction is significant because 4-aminophenol is far less toxic, more biodegradable, and serves as a valuable intermediate in pharmaceutical and chemical synthesis, thereby illustrating both environmental remediation and resource recovery [14].

One managing technique for nitrophenol contamination is photocatalytic reduction. In this sense, metallic nanoparticles are fundamental for their environmental compatibility and their catalytic efficacy [16]. Most of the research has been focused on noble metal alloy nanoparticles, while there is little research on transition metal nanoparticles, particularly bimetallic pairs [17, 18]. Due to their unique properties, bimetallic nanoparticles have many potential applications, for instance, in catalysis and antibacterial activity. Recent studies have shown that Fe/Ru and Ag-Pd nanoparticles are more efficient in these respects [19, 20].

This study aims to fill in this research gap by sustainably synthesising Cu, Fe, and Cu/Fe nanoparticles using *K. senegalensis* extract. Besides determining the photocatalytic capacity of the green-synthesised nanoparticles to reduce 4-NP and their antibacterial activity against some pathogens. This research seeks to focus on urgent and significant health and environmental challenges while paving the way for positive advancements in the synthesis of nanoparticles.

2. MATERIALS AND METHODS

2.1. PLANT MATERIAL COLLECTION, IDENTIFICATION AND AUTHENTICATION

K. senegalensis was obtained from Mararaba-Lafia, Nasarawa State, Nigeria, and was utilised for the synthesis of metallic nanoparticles via a green route method. Plant identification was carried out at the Federal University of Lafia, Department of Botany and Plant Science, herbarium unit, and afterwards, the plant was prepared for laboratory phytochemical analysis and the synthesis of the nanoparticles.

2.2. PLANT EXTRACT PREPARATION

After being cleaned with double-distilled water to get rid of dust and debris, *K. senegalensis* leaves were allowed to air dry for two to three days. A blender was used to grind the dried leaves into a fine powder. For three days at room temperature with periodic shaking, 10 g of the leaf powder was soaked in 100 mL of double-distilled water. Whatman No. 1 filter paper was then used to

filter the resultant solution [21]. Until it was needed again, the concentrated extract was kept at 4 ˚C.

2.3. PHYTOCHEMICAL SCREENING OF AQUEOUS PLANT EXTRACT

2.3.1. Test for tannins

A few drops of 0.1% $FeCl_3$ were added to filtered mixtures of 5 g of the samples and 20 mL of distilled water. A colour change from brownish green or a blue-black colouration was observed and was taken as evidence for the presence of tannins [22].

2.3.2. Test for saponins

The froth and emulsion tests were applied. The screening test was based on saponins' capacity to form an emulsion with oil. In a water bath, 2 g of the material were cooked for 5 min in 25 mL of distilled water before being filtered. 5 mL of distilled water were combined with 10 mL of the filtrate, and the mixture was agitated vigorously to create froth. Froth was combined with three drops of olive oil, agitated briskly, and the formation of an emulsion was monitored [23].

2.3.3. Test for flavonoids

To obtain the filtrate, 5 g of the materials were suspended in 100 mL of distilled water. Ten milliliters of filtrate were mixed with around five milliliters of diluted ammonia solution, and then a few drops of concentrated H_2SO_4 were added. The yellow coloring indicated the presence of flavonoids [23].

2.3.4. Test for terpenoids

3 mL of concentrated H_2SO_4 were carefully added to create a layer after 5 mL of each extract had been combined with 2 mL of chloroform. Terpenoids were present because the contact developed a reddish-brown coloring [24].

2.3.5. Test for sterols

2 mL of each extract was mixed with 2 mL of concentrated H_2SO_4. The presence of sterols was indicated by a red colouring [22].

2.3.6. Test for alkaloids

To check for alkaloids, the Mayer, Dragendroff, Wagner, and picric acid tests were employed. In a steam bath, 1 g of the plant material was cooked with 5 mL of 2% hydrochloric acid for nearly two minutes before being filtered. Two drops of Mayer's and Wagner's reagent were added to one millilitre of the filtrate. The presence of alkaloids was demonstrated by turbidity or precipitation with either of the reagents [25].

2.3.7. Test for glycosides

5 mL of aqueous extract in glacial acetic acid were mixed with a few drops of $FeCl_3$ and concentrated sulphuric acid. Glycosides are indicated by a bluish-green hue in the top layer and a reddish-brown colouring at the intersection of two layers [22].

2.4. GREEN SYNTHESIS OF IRON OXIDE NANOPARTICLES

The procedure by Ref. [26] was slightly modified to create Fe-based nanoparticles by adding 0.5 M $Fe(NO_3)_3{\cdot}9\,H_2O$ to aqueous *K. senegalensis* extracted in a 1:5 volume ratio. A colloidal suspension was obtained by stirring the mixture for 60 min and then letting it stand at room temperature for an additional 30 min. The Fe_3O_4-NPs were obtained by centrifuging the mixture, washing it with ethanol many times, and then vacuum-drying it at 40 ˚C.

2.5. GREEN SYNTHESIS OF COPPER OXIDE NANOPARTICLES

A solution of 0.2 M aqueous $Cu(NO_3)_2.3H_2O$ was made and kept in brown bottles. 400 mL of 0.2 M $Cu(NO_3)_2.3H_2O$ solution was gradually added dropwise to 100 mL of plant leaf extract while being continuously stirred. For 24 hours, the mixture was incubated at room temperature. At 30- and 60 min intervals, the colour change was monitored. The solution was centrifuged for 15 min at 10000 rpm when the colour changed from blue to light brownish, which visually shows the synthesis of CuO NPs. To get rid of contaminants, the produced CuO NPs were cleaned with ethanol and deionised water [27, 28]. The NPs were dried before being crushed for use in additional analysis.

2.6. SYNTHESIS OF BIMETALLIC COPPER AND IRON OXIDE NANOPARTICLES

10 mL each of 0.2 M $Fe(NO_3)_3.9H_2O$ and 0.2 M $Cu(NO_3)_2{\cdot}3H_2O$ salts were dissolved in 80 mL of deionized water in 250 mL beaker. Filter paper filtration was used to eliminate the contaminants once the salts had fully dissolved. 100 mL of extract was added dropwise to the 100 mL Fe (II)/Cu (II) mixture to develop the synthesis of CuO/Fe_2O_3-NPs. When several drops of *K. senegalensis* extract were added, the mixture's color progressively changed from yellow to brown to black, indicating that the metals' equivalents were reduced to zero-valent and that CuO/Fe_2O_3-NPs synthesis was finished. This procedure has also been reported in the recently published work from our lab [29].

2.7. CHARACTERIZATION OF CuO, Fe_2O_3 AND CuO/Fe_2O_3 NANOPARTICLES

A UV-visible spectrophotometer (Biochrom Libra PCB 1500 UV-VIS spectrophotometer model) was used to determine the wavelength with the highest absorbance of the mono and bimetallic nanoparticles by dispersing them in a 1 cm path length quartz cuvette, and the wavelength scan was performed to obtain a stable absorbance at the maximum wavelength. UV-Vis spectra between 300 nm and 700 nm were used to identify the monometallic and bimetallic nanoparticles' surface plasmon resonance (SPR) peak. The XRD analysis of the synthesized nanoparticles powders were performed on Phillips PW 1820 X-ray diffractometer at a scan rate of 0.064 s^{-1}, in the 2θ range from 5˚ to 90˚ with monochromatized Cu Kα (λ = 1.5406 nm) radiation to determine their crystalllinity. The PerkinElmer Spectrum and Fourier Transform Infrared (FTIR) spectrometer (PerkinElmer, Inc., Waltham, Massachusetts, USA) was used to identify the functional groups of the phytochemicals in the aqueous plant extract that enabled the bio-reduction of salt ions in the 500 cm^{-1} to 4000 cm^{-1} range. High-Angle Annular Dark-Field Scanning Electron Microscopy (HAADF STEM) was used to examine the morphology of the nanoparticles (STEM-LEO S1430 VP from M/S LEO Electron Microscopy Ltd, Cambridge, UK and UHR FE-SEM Carl Zeiss ULTRA Plus, Carl Zeiss Meditec AG, Jena,

Germany) [28, 29].

2.8. 4-NITROPHENOL CATALYTIC REDUCTION USING CuO, Fe_2O_3, AND CuO/Fe_2O_3 NANOPARTICLES AS NANO CATALYSTS

To examine the catalytic activity of the as-synthesized nanoparticles and determine how quickly sodium borohydride can reduce 4-nitrophenol, the reduction of 4-NP by $NaBH_4$ was selected as a model reaction. Usually, the reaction was conducted in a quartz cuvette and observed at room temperature (298 K) using UV-vis spectroscopy. To improve concentration, all of the produced samples were appropriately diluted with distilled water. Thus, an aqueous solution of sodium borohydride was combined with the freshly made 10 mM 4-nitrophenol. A bright yellow solution formed when 1.0 mL of aqueous 4-NP solution was combined with 0.35 mL of 0.1 mM $NaBH_4$. Following that, deionized water was used to disperse metal oxides, including CuO, Fe_2O_3, and CuO/Fe_2O_3, respectively. The generated yellow solution in each of the monometallic and bimetallic oxide nanoparticles was mixed with 2.14 mL of the 4-nitrophenol and sodium borohydride solution. UV-vis absorption spectroscopy was used to measure the reaction's progress at intervals of 0.5 min, 1.0 min, 1.5 min, 2.0 min, 2.5 min and 3.0 min, respectively, within a scanning range of 200 nm to 800 nm. It was observed that the solution's color gradually disappeared as the reaction went on [27, 29].

2.9. ANTIBACTERIAL ASSAY

2.9.1. Zone of inhibition

The agar-well diffusion method, as outlined by Refs. [30, 31], was used to examine the as-synthesized nanoparticles' antibacterial efficacy. Bacterial isolates were cultivated in nutritional broth for 12–18 h, encompassing both Gram-positive (*Bacillus subtilis*) and Gram-negative (*Escherichia coli* and *Pseudomonas aeruginosa*) microorganisms. Following this time, the inoculum was standardized to 0.5 McFarland standards, which is equivalent to 10^6 cfu/mL. The agar medium was punctured with wells of 6 mm in diameter and filled with equal amounts of solutions of CuO/Fe_2O_3 bimetallic nanoparticles at different concentrations (10 µg/mL, 20 µg/mL, 30 µg/mL and 40 µg/mL) on Mueller-Hinton agar plates (Hi Media) after 100 µL of the standardized cell suspensions had been spread out on the agar surface. A zone of inhibition was checked for on the plates following a 24 h incubation period at 37 °C.

2.9.2. Bacterial strains and culture conditions

Gram-positive *Bacillus subtilis* and Gram-negative strains of *Escherichia coli* and *Pseudomonas aeruginosa* were among the test microorganisms. CLSI criteria were followed in the maintenance of the cultures [32, 33]. For normal growth and maintenance, Mueller-Hinton Broth (MHB) and Agar (MHA) were utilized, and for biofilm development, Tryptic Soy Broth (TSB) supplemented with 1% glucose was employed. For 24 h, all strains were incubated aerobically at 37 °C. Overnight cultures were used to create bacterial suspensions for the tests, which were then corrected to a 0.5 McFarland standard in sterile water.

2.9.3. Minimum inhibitory concentration (MIC) assay

Using broth microdilution, the antibacterial activity of CuO/Fe_2O_3 bimetallic nanoparticles was assessed. Each well in a 96-well plate received 100 µL of MHB, which was followed by 100 µL of either the nanoparticle solution (in DMSO) or controls (DMSO as a negative control, Vancomycin for Gram-positive, and Norfloxacin for Gram-negative) at an initial concentration of 1 mg/mL. After performing successive two-fold dilutions (500 µg/mL to 0.49 µg/mL), 10 µL of bacterial inoculum was added to every well. The plates were incubated for 24 h at 37 °C. Absorbance at 620 nm was used to measure bacterial growth. Three duplicates of each test were run [32, 33].

2.9.4. Minimum bactericidal concentration (MBC) determination

Following MIC analysis, samples from wells exhibiting no discernible growth were plated onto MHA plates to estimate MBC. In comparison to the control, the MBC was found to be the lowest concentration that produced a reduction in viable colonies of > 99.9%. For every strain, testing was conducted three times [32, 33].

2.9.5. Minimum biofilm inhibitory concentration (MBIC)

In a 96-well plate, biofilm inhibition was measured using TSB and 1% glucose. 20 µL of bacterial suspension was injected and statically incubated for 24 h at 37 °C following the addition of nanoparticle dilutions (using the same range and technique as MIC). After removing non-adherent cells with PBS, biofilms were fixed for an hour at 60 °C and stained for 15 min with 1% crystal violet. Following rinsing, ethanol was used to dissolve the bound dye, and absorbance at 595 nm was recorded. In comparison to untreated controls, the percentage suppression of biofilm formation was computed. Three duplicates of each assay were carried out, and the results were statistically represented as mean ± standard deviation [32, 33].

$$\text{Biofilm Formation (\%)} = \frac{\text{OD}_{595} \text{ of the test well}}{\text{OD}_{595} \text{ of non-treated control well}} \times 100. \quad (1)$$

2.10. DATA ANALYSIS

Machine data obtained from UV-Vis, FTIR, STEM were plotted using Origin Pro 2020 graphing and analysis software.

3. RESULTS AND DISCUSSION

3.1. PHYTOCHEMICAL COMPOSITION OF *K. senegalensis*

Saponins, alkaloids, flavonoids, tannins, steroids, and terpenoids were found in *K. senegalensis* after a preliminary screening of its phytochemical content. Tannins were found to be strongly present, while saponins, flavonoids, alkaloids and steroids were moderately present. Terpenoids were the least present, while glycosides were found to be absent.

3.2. CHARACTERISTICS OF CuO, Fe_2O_3 AND CuO/Fe_2O_3 NANOPARTICLES

3.2.1. UV-visible spectroscopy analysis

Metallic nanoparticles show absorbance in the UV-Vis region; hence, UV-Vis spectrophotometric examination was utilised as

Table 1. Phytochemicals of *K senegalensis*.

Parameters	Qualitative analysis
Alkaloids	++
Flavonoids	++
Saponins	++
Tannins	+++
Steroids	++
Terpenoids	+
Glycosides	–

+++ strongly present, ++ moderately present, + least present, – absent.

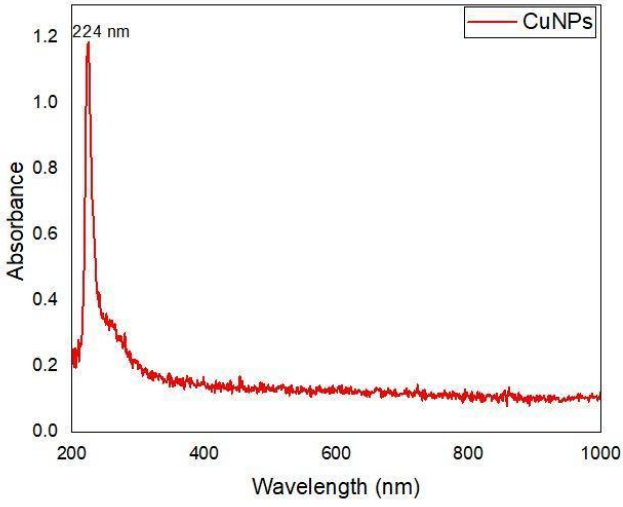

Figure 1. UV-vis spectrum of CuO nanoparticles.

an immediate preliminary test for the confirmation of nanoparticle formation. The UV-Visible absorption spectrum shown in Fig. 1 demonstrates the optical properties of CuO NPs. A prominent absorption peak is observed at 224 nm, which is characteristic of CuO NPs. This peak arises due to the electronic transitions within the CuO nanoparticles, specifically the charge transfer transitions between the copper and oxygen atoms in the CuO lattice. The absorption peak at 224 nm matches the findings of Ref. [34], confirming the consistency of the optical behavior of CuO NPs in various studies. This agreement validates the production method utilized in the present study and demonstrates that the nanoparticles have the anticipated optical characteristics. Furthermore, as is typical for CuO NPs, the absorbance gradually decreases following the peak, suggesting that light interacts with the nanoparticles less at higher wavelengths.

The optical features observed in Fe_2O_3 NPs are shown in Fig. 2. There is an obvious absorption peak at 290 nm. This peak can be attributed to the specific electronic transitions in the Fe_2O_3 NPs and the structural interactions between the iron and oxygen. Notably, the spectrum does not contain any further peaks. This clearly indicates that there are no measurable contaminants influencing the absorbance of the nanoparticle, confirming its purity. The spectrum clearly highlights the extent to which the synthesis process worked. The identity and behavior of the Fe_2O_3 nanoparticles are supported by this particular absorption property, which is consistent with earlier studies [35]. Beyond 290 nm, the absorbance gradually decreases, illustrating the limited interaction of light with the particles at higher wavelengths. This feature is in line with what is expected based on the bandgap energy of the material, thus, it can be linked to the bandgap energy of Fe_2O_3, arising from the absorption spectrum.

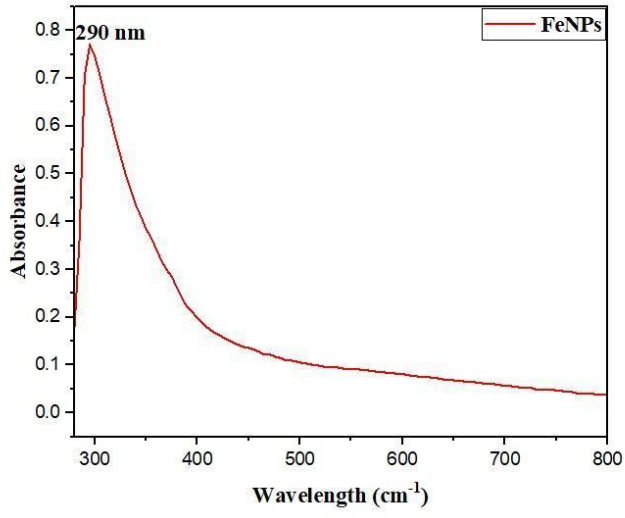

Figure 2. UV-vis spectrum of Fe_2O_3 nanoparticles.

The UV-visible spectroscopy analysis of CuO/Fe_2O_3 (NPs) has been reported in the recently published work from our lab [29].

3.2.2. FTIR analysis

The functional groups on the generated metallic oxide nanoparticles were identified using FTIR spectroscopy. The compounds and their functional groups that were present in the samples were identified using FTIR characterisation. Several unique absorption bands that correlate to particular functional groups and chemical bonds can be seen in the CuO NPs' infrared spectrum. The range from 3282 cm^{-1} indicates the presence of surface bound hydroxyl functionalities. This characteristic is pivotal as it generally affects the reactivity of the nanoparticles and their interaction with their environment. The peak at 2965 cm^{-1} is attributed to carboxylic acid groups, which may originate from some organic residues or stabilising agents employed during the synthesis.

The band at 1625 cm^{-1} corresponds to carbonyl groups (C=O stretching). This feature is typical of ketones or aldehydes [35]. It provides insight into the potential interactions and chemical composition of CuO NPs. Additionally, the band at 1065 cm^{-1} suggests the presence of unsaturated organic molecules or structural elements in the nanoparticles, as it is indicative of C=C bonds [35, 36].

The spectrum also shows bands in the lower wavenumber region. These bands are important for identifying oxide phases. Bands between 500 cm^{-1} and 810 cm^{-1} are associated with magnetite. Bands between 620 cm^{-1} and 660 cm^{-1} relate to maghemite. In addition, bands at 470 cm^{-1} and 540 cm^{-1} are typical of hematite, as noted by [36]. These features help us understand the crystalline phases and structural makeup of CuO

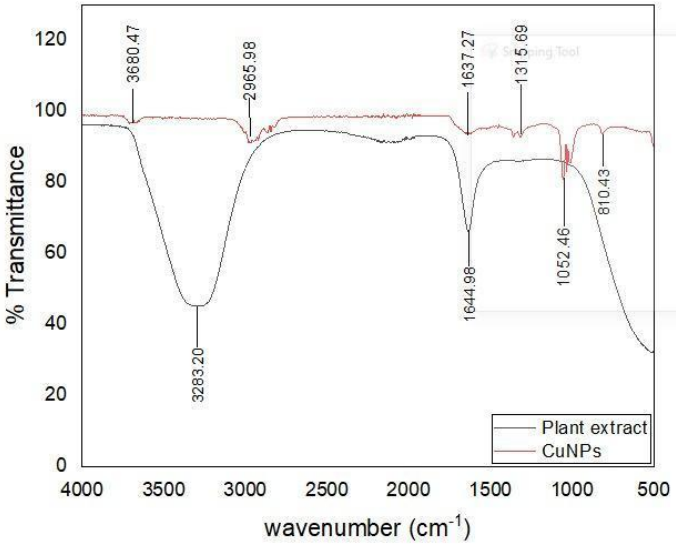

Figure 3. FTIR spectra of CuO nanoparticles.

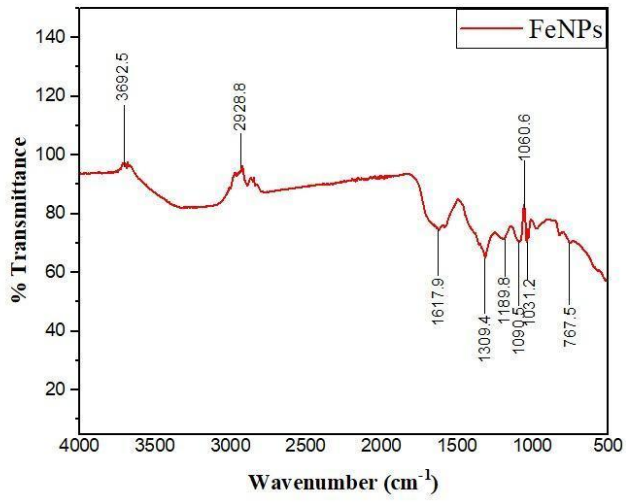

Figure 4. FTIR of Fe_2O_3 NPs.

NPs. The FTIR spectrum not only confirms the presence of CuO nanoparticles but also offers further explanation about their functional groups and structural characteristics.

The FTIR showing the functional groups in the Fe_2O_3 NPs is shown in Fig. 4. The broad band at 3692.5 cm^{-1} in the FTIR spectra of the Fe_2O_3 NPs is associated with the surface O-H group, which is linked to phenolic compounds. Since the compound had a C-H stretching vibration and the -CH_2 functional groups were as reported by Refs. [5, 37], the bands that were seen at wave numbers of 2928.8 cm^{-1} were attributed to C-H. The band at 1617.9 cm^{-1} was identified as the ketone group from dimerized saturated aliphatic acids which is C=O, as described by [38]. The C-O stretching in carboxyl groups was identified as the cause of the bands at 1309.4 cm^{-1}. The stretching vibration of an alkyl amine is symbolized by the band at 1189.8 cm^{-1}.

The bands at 1060 cm^{-1} to 1031.2 cm^{-1} stretching vibration were attributed to C-O groups [39]. The band 767.5 cm^{-1} represents Fe-O nanoparticles, which corresponds to the alkyl halides stretching vibration in metals [40]. The FTIR analysis of CuO/Fe_2O_3 NPs has been reported in the recently published work from our lab [29].

3.2.3. HAADF STEM analysis

The HAADF STEM image of CuO NPs is presented in Fig. 5. The particles are evenly distributed and have an average size of 20 nm, according to the photograph. By detecting elemental contrast, the HAADF STEM approach offers information about the distribution and shape of the nanoparticles. The spherical shape and even distribution of the CuO particles are shown by the significant contrast between them and the surrounding medium when utilizing the annular dark-field imaging mode. These characteristics are crucial for electronics and catalysis applications. Reliable performance is the result of stable particle sizes and uniform distribution. A high surface area is also indicated by a tiny particle size in reactions that need surface activity.

The mean grain size for the Fe_2O_3 NPs is 50 nm as determined from the HAADF STEM image (Fig. 6). The larger size

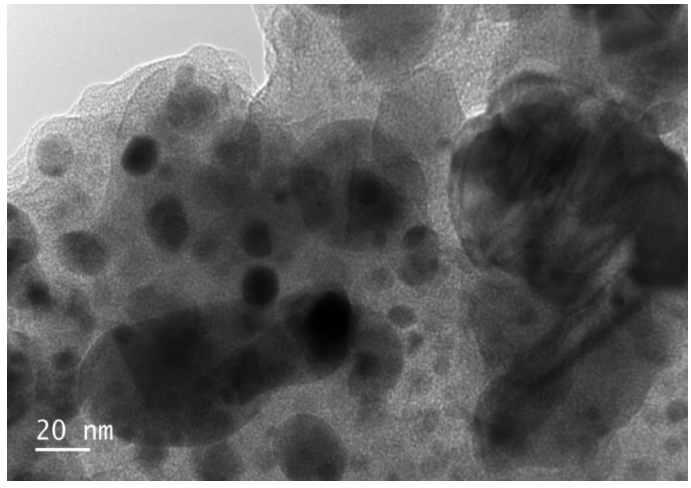

Figure 5. HAADF STEM images of CuO NPs.

for Fe_2O_3 NPs, contrasted with the CuO NPs, may alter their physical and chemical properties as the larger size CuO particles implies a lower surface area, and therefore, the Fe_2O_3 NPs will have a smaller surface area for the adsorption, catalysis and other surface-related chemical processes. The Fe_2O_3 NPs are HAADF STEM characterised which denotes their uniformity in composition and the structural stability of the particles. Our lab published CuO/Fe_2O_3 NPs HAADF STEM analysis in Ref. [29].

3.3. X-RAY DIFFRACTION (XRD) ANALYSIS OF THE SYNTHESIZED NANOPARTICLES

The XRD patterns of the green synthesized CuO, Fe_2O_3 and CuO/Fe_2O_3 NPs (Figure 7) were studied to determine the fabrication of highly crystalline metal oxides phases. The CuO and Fe_2O_3 NPs displayed a sharp monoclinic tenorite and rhombohedral haematite, respectively, indicating excellent phase purity for the two metal oxides. The CuO/Fe_2O_3 NPs diffraction showed the heterostructural diffractions of both metals without any impurity phases instead of the single phases. The average crystalline sizes of the CuO, Fe_2O_3 and CuO/Fe_2O_3 NPs were as-

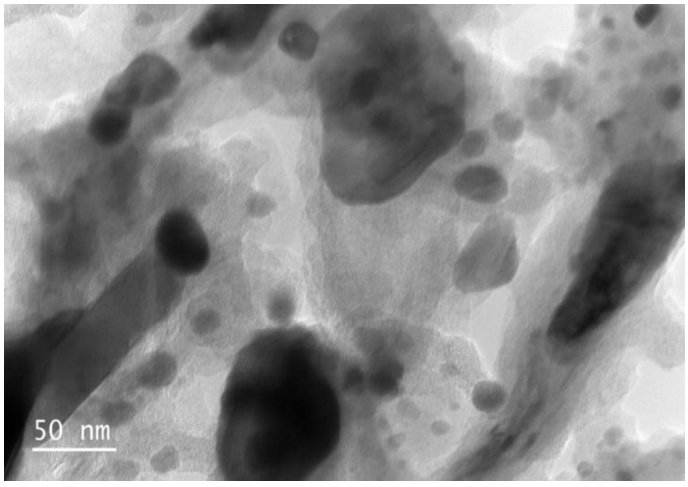

Figure 6. HAADF STEM images of Fe_2O_3 NPs.

certained using the Scherrer equation and taking the full width at half maximum (FWHM) of the most intense peaks around 2 theta at 38°. The crystallite sizes of CuO, Fe_2O_3 and CuO/Fe_2O_3 NPs were found to be 26, 22 and 28 nm, respectively. The XRD results show that green synthesized metal oxides exhibited a sharp phase-pure nanoscale and highly crystalline NPs for antimicrobial and catalytic applications [41, 42].

3.4. CATALYTIC REDUCTION OF 4-NITROPHENOL (4-NP) TO 4-AMINOPHENOL (4-AP)

The need to convert 4-nitrophenol to 4-aminophenol is hinged on the fact that 4-aminophenol is a key precursor for the manufacture of acetaminophen (paracetamol), one of the most widely used analgesic and antipyretic drugs globally. The direct hydrogenation of 4-NP to 4-AP provides a cleaner and more efficient route to this essential pharmaceutical compound compared to older multi-step processes that generated more waste. As demonstrated by control experiments, sodium borohydride by itself is not efficient in reducing 4-nitrophenol (4-NP) [41]. The catalytic reduction was greatly enhanced by the addition of CuO nanoparticles. The uniform dispersion and substantial surface area of the CuO NPs promote electron transport and enhance catalytic activity. After 1.0 min, the mixture of CuO NPs and sodium borohydride (0.5 ml) was added to 4-NP, thereby reducing 4-NP as shown in Figure 8a. Consequently, the same operation was performed at 2.0 min for the blue curve, which was reduced from green. After 3.0 min, the 4-NP was completely reduced (purple curve) on the graph. This shows that CuO NPs and $NaBH_4$ have the capacity to convert 4-NP to 4-AP after 3 minutes. The time-dependent study of the UV absorption of the CuO NPs catalyst with sodium borohydride causes a significant reduction.

The synthesized nanoparticles accelerated the reduction of nitrophenol through a Langmuir–Hinshelwood mechanism, where both nitrophenolate ions and BH_4^- co-adsorb on the nanoparticle surface to enable rapid electron transfer [41]. Their high surface area and surface defects facilitate hydride activation and lower the activation energy for conversion to aminophenol. Although metallic or metal-oxide nanoparticles may theoretically generate oxidizing species, the strongly reducing environment of excess

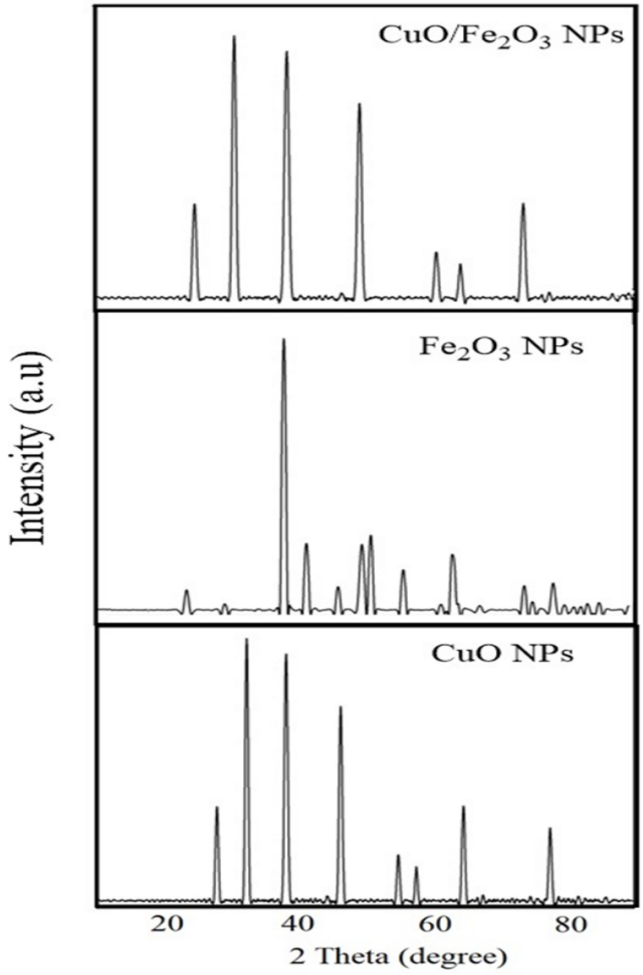

Figure 7. XRD patterns of CuO, Fe_2O_3 NPs and CuO/Fe_2O_3 NPs nanoparticles.

$NaBH_4$ suppresses such pathways. Consequently, the nanoparticles remain in a reduced, catalytically active state, promoting efficient nitrophenol reduction rather than hindering it.

In the catalytic reduction of nitrophenols, the excellent performance of the catalyst is attributed to the uniform distribution of nanoparticles on the support surface. The reduction of 4-nitrophenol (4-NP) occurs within 2.5 minutes. 4-NP is shown by the red curve in Figure 8b, which has a distinct UV-visible spectrum peak at 400 nm. The 4-NP solution was mixed with 0.5 ml of $NaBH_4$ and Fe_2O_3 NPs at 1.0 min. This resulted in an apparent change in color from yellow to blue. The green curve indicates that the identical combination was applied again at 2.0 minutes. Thereafter, a new peak appeared in the UV-visible spectrum that moved down to 380 nm. By 2.5 mins, the reduction was complete, indicated by a light green colour. This demonstrates the capability of Fe_2O_3 NPs and $NaBH_4$ to effectively convert 4-NP to 4-aminophenol.

The bimetallic nanoparticles had the perfect reduction of 4-NP to 4-AP coupled with sodium borohydride. As described in the catalytic reduction of 4-nitrophenols, the excellent performance of the catalyst is due to the uniform distribution of nanoparticles on the support surface. The red curve, as indicated in Figure 8c, was 4-NP with a sharp peak of UV-visible at 300 nm. At 0.5

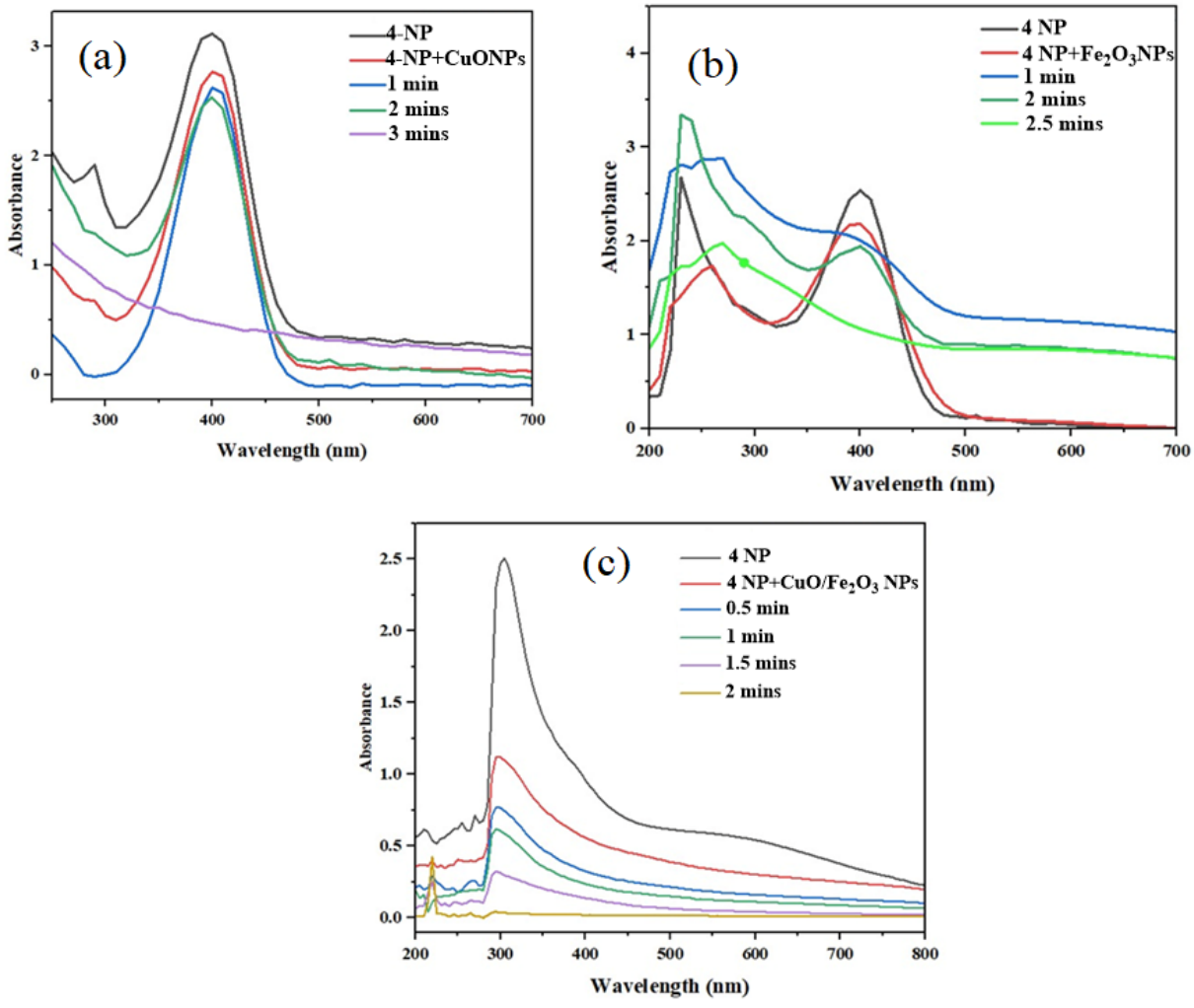

Figure 8. Catalytic reduction of 4-nitrophenol to 4-aminophenol using $NaBH_4$ and (a) CuO NPs (b) Fe_2O_3 NPs (c) CuO/Fe_2O_3 NPs.

min, which indicated the blue curve, the mixture of CuO/Fe_2O_3 NPs and $NaBH_4$ at 0.5 ml was added to 4-NP, thereby reducing the effect of the 4-NP. Consequently, the same operation was performed at 1.0 min for the green curve and 1.5 minutes for the purple curve, respectively (Figure 8c). At 2.0 mins, which is the yellow curve, the sharp peak disappeared, which shows a complete reduction. This shows that the effect of the combined catalyst with sodium borohydride brings a better result on the reduction of 4-nitrophenol to 4-aminophenol. The catalytic reduction of 4-nitrophenol to 4-aminophenol proceeds via a surface-mediated hydrogenation mechanism where borohydride ions decompose on the catalyst surface to generate reactive hydrogen species. For the monometallic systems, semiconducting CuO nanoparticles act as an electron relay, utilizing Cu^+/Cu^{2+} redox cycling to facilitate reduction, while Fe_2O_3 is significantly less active due to its inferior capacity for borohydride activation and electron transfer [41]. However, in a CuO/Fe_2O_3 bimetallic nanocomposite, a synergistic interfacial effect dominates: a heterojunction is formed, causing electron transfer to the CuO phase, which creates an electron-rich surface that dramatically enhances borohydride decomposition and hydrogen generation, thereby accelerating the sequential hydrogenation of the nitro group and resulting in superior catalytic performance [41].

3.5. ANTIMICROBIAL ASSAY

3.5.1. Zone of inhibition (antimicrobial effectiveness test)

The Agar well diffusion method was used to evaluate the antibacterial activity of CuO/Fe_2O_3 nanoparticles produced by *K. senegalensis* against *Escherichia coli*, *Bacillus subtilis*, and *Pseudomonas aeruginosa*. CuO/Fe_2O_3 shown notable concentration-dependent action against both Gram-positive and Gram-negative bacteria (Table 2, Figure 9). Against *Escherichia coli*, the CuO/Fe_2O_3 nanoparticles produced a concentration-dependent response, up to 14 mm at 40 μg/ml. This surpasses the amoxicillin (12 mm) positive control. This suggests a synergistic interaction between the copper and the iron oxides. Similar superiority was recorded against *Bacillus subtilis*, where CuO/Fe_2O_3 gave a 15 mm response and closer to amoxicillin (16 mm). This could be attributed to the dual action of the Cu^{2+} and Fe^{3+} ions intensifying oxidative stress through the ROS generation and enhanced cell wall penetration [42], especially when the functionality present on the CuO/Fe_2O_3 nanoparticles, as shown in the FTIR spectra, stabilises and functionalizes the particles [29]. In contrast, CuO/Fe_2O_3 nanoparticles showed limited inhibitory ac-

Table 2. Antibacterial effects of different concentrations of synthesized CuO/Fe_2O_3 nanoparticles against the tested bacteria.

Test organism	Zone of inhibition (mm)				
	10	20	30	40	Amoxicillin (25 μg/ml)
Escherichia coli	6	7	12	14	12
Bacillus subtilis	6	6	6	15	16
Pseudomonas aeruginosa	8	10	9	9	8

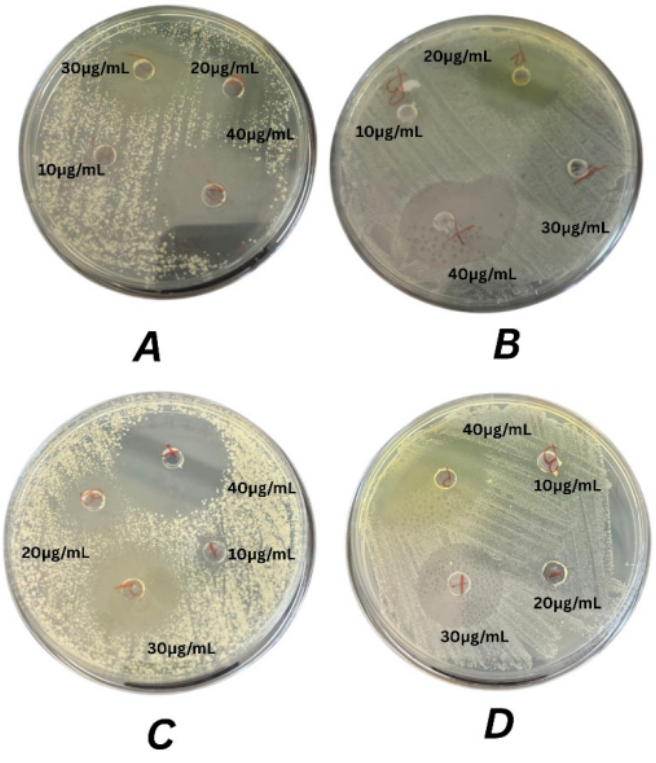

Figure 9. The zone of inhibition test measures the effect of CuO/Fe_2O_3 nanoparticles at different concentrations (10, 20, 30, and 40 μg/ml) on the bacterial strains (A) *E. coli*, **(B)** *Bacillus subtilis*, **and (C)** *Pseudomonas aeruginosa* **(D) The positive control was amoxicillin at 25 μg/ml.**

tivities against *Pseudomonas aeruginosa*, a pathogen known for its multidrug resistance. The CuO/Fe_2O_3 nanoparticles showed a maximum zone of 10 nm. This could be attributed to *Pseudomonas aeruginosa* robust defence mechanism, which involves efflux pumps, thick exopolysaccharide layers and antioxidant enzymes that neutralise ROS [43]. While the bimetallic nanoparticles showed modest advantages, their efficacy was insufficient to overcome the intrinsic resistance strain.

3.5.2. Minimum inhibitory concentration (MIC)

The green-synthesised CuO/Fe_2O_3 bimetallic nanoparticles shown remarkable antibacterial activity against both Gram-positive and Gram-negative bacteria, according to the MIC data shown in Table 3. The MIC of CuO/Fe_2O_3 for *Escherichia coli* and *Bacillus subtilis* was low, at 8.00 μg/ml. Compared to the common antibiotics norfloxacin (8.25 μg/ml) and vancomycin (8.50 μg/ml), these values are somewhat better. A synergistic impact between copper and iron oxides was demonstrated by the decreased MICs of CuO/Fe_2O_3, which improved the NPs' capacity to rupture microbial membranes and suppress metabolic activity at comparatively low concentrations. For *Pseudomonas aeruginosa*, the MIC of CuO/Fe_2O_3 reached 40.00 μg/ml, higher than Norfloxacin (16.00 μg/ml). This result suggest a moderate inhibitory effect of the CuO/Fe_2O_3 nanoparticles is likely due to the combined ROS generation through Fe^{3+} and Cu^{2+} ions mediated Fenton-like reactions. While CuO disrupts protein and DNA via oxidative process, Fe_2O_3 aids the ROS propagation within the bacterial cells, leading to potent and antimicrobial mechanisms [44].

Table 3. The minimum inhibitory concentration (MIC) and minimum bactericidal concentration (MBC) of the CuO/Fe_2O_3 bimetallic nanoparticles in μg/ml. Data represent the median values of three replicates.

Test organism	Nanoparticles	MIC	MBC
Gram-positive			
Bacillus subtilis	CuO/Fe_2O_3 Nanoparticles	8	16
	Vancomycin (Control)	8.5	17
Gram-negative			
Escherichia coli	CuO/Fe_2O_3 Nanoparticles	8	16
	Norfloxacin (Control)	8.25	16.5
Pseudomonas aeruginosa	CuO/Fe_2O_3 Nanoparticles	40	80
	Norfloxacin (Control)	16	32

3.5.3. Minimum bactericidal concentration (MBC)

The MBC results in Table 3 further support the bactericidal potential of the synthesized nanoparticles. For both *Bacillus subtilis* and *Escherichia coli*, CuO/Fe_2O_3 showed MBCs of 16.00 μg/ml, which doubles their MICs, indicating its bactericidal action rather than bacteriostatic [45]. This indicate the enhanced killing efficiency of the CuO/Fe_2O_3 nanoparticle formulation. These are similar to the ones obtained for Norfloxacin (16.50 μg/ml) and Vancomycin (17.00 μg/ml), suggesting that CuO/Fe_2O_3 can serve as a viable substitute in clinical diagnosis. The most resistant organism, *Pseudomonas aeruginosa*, requires a higher MBCs. CuO/Fe_2O_3 gave MBC of 80.00 μg/ml confirming bactericidal activities. The increased dosage required for *Pseudomonas aeruginosa* reflects its known resistance mechanism, which include biofilm formation and reduced permeability [46]. However the ability of CuO/Fe_2O_3 to exhibit 2-fold MIC-MBC relationship support its potential as antimicrobial agent.

3.5.4. Minimum biofilm inhibitory concentration (MBIC)

The MBIC values of the synthesized nanoparticles are presented in Table 4. The CuO/Fe_2O_3 showed the most promising activity. The MBIC for *Bacillus subtilis* was 16.00 μg/ml, achieving 52% inhibition, while for *Escherichia coli* it was 32.00 μg/ml, with 55% inhibition. Considering the extracellular polymeric substances (EPS) matrix of a biofilm functions as a strong physical and chemical barrier, limiting the penetration and efficacy of antimicrobial drugs, it is typical and expected that these values are larger than the corresponding MICs [47]. The fact that the nanoparticles could achieve over 50 % inhibition of biofilm formation at these relatively low concentrations underscores their potential to disrupt the initial stages of biofilm development. At an MBIC of 160.00 μg/ml for the highly resistant *Pseudomonas aeruginosa*, 50% inhibition was noted for CuO/Fe_2O_3. The control antibiotic, norfloxacin, had an MBIC of 64.00 μg/ml and

Table 4. Minimum biofilm inhibitory concentration (MBIC) of the synthesized CuO, Fe_2O_3, and CuO/Fe_2O_3 nanoparticles in μg/ml, showing the respective concentration and % inhibition (Data represents the median values of three replicates).

Test organism	Nanoparticles	MBIC (μg/ml)	% Inhibition at MBIC
Gram-positive			
Bacillus subtilis	CuO/Fe_2O_3 Nanoparticles	16	52%
	Vancomycin (Control)	17	51%
Gram-negative			
Escherichia coli	CuO/Fe_2O_3 Nanoparticles	32	55%
	Norfloxacin (Control)	33	54%
Pseudomonas aeruginosa	CuO/Fe_2O_3 Nanoparticles	160	50%
	Norfloxacin (Control)	64	75%

displayed 75% inhibition. This indicates that, on the biofilm formation inhibition front, norfloxacin surpassed the performance of the nanoparticles in this study for the biofilm formation inhibition of P. *aeruginosa*. This aligns with earlier reports that *P. aeruginosa* biofilm are highly resilient due to low membrane permeability and efficient efflux pump systems [47]. These findings aligned with recent studies supporting the enhanced antibiofilm activity of multimetallic nanocomposites over monometallic systems. For instance, CuO-ZnO nanoparticles using a greener approach have been reported to inhibit over 60 % of *E.coli* biofilm at concentrations of 25-50 μg/ml [48]. The performance of control antibiotics vancomycin and norfloxacin is compared with the μg/ml values of the MIC, MBC, and MBIC for the CuO/Fe_2O_3 nanoparticles against *Bacillus subtilis, Escherichia coli*, and *Pseudomonas aeruginosa*.

4. CONCLUSION

This study establishes a scalable, eco-conscious strategy for the fabrication of multifunctional CuO, Fe_2O_3, and CuO/Fe_2O_3 nanoparticles via a green synthetic route utilizing *Khaya senegalensis* phytochemicals. The successful integration of plant-derived reductants and stabilizers yielded monodispersed nanoparticles with tailored optical, structural, and surface features conducive to high catalytic and antimicrobial efficacy. The CuO/Fe_2O_3 bimetallic composite was the most promising of the nanostructures that were produced. In less than two minutes, 4-nitrophenol was rapidly reduced. The efficient contact between the Cu and Fe oxide surfaces, which permits rapid electron transfer, is responsible for the observed result. These nanoparticles significantly suppressed biofilms and demonstrated minimum inhibitory concentration (MIC) and minimum bactericidal concentration (MBC) values that were equal with or higher than those of conventional antibiotics in tests for antibacterial activity. The bimetallic CuO/Fe_2O_3 nanoparticles exhibited excellent results with *Bacillus subtilis* and *Escherichia coli*, representing better performances, specifically, the benefits of bimetallic compositions in bolstering antimicrobial activity, thereby illustrating the potential of bimetallic compositions as a promising green nanotechnology pathway to tackle ubiquitous and tenacious pathogens. More research will attempt to create surface functionalisation to allow better selectivity, biocompatibility, and targeted delivery to the pathogens.

DATA AVAILABILITY STATEMENT

The data supporting the findings of this study are available within the article. Raw data, including synthesis parameters, characterization results, and biological activity assays, can be accessed upon request from the corresponding author.

ACKNOWLEDGMENT

This research was funded by the Tertiary Education Trust Fund (TETFund) of the Federal Republic of Nigeria through the Institutional Base Research Fund 2025 (Award Letter Reference Code: FUL/REG/TETFund/002/VOL.V1/321) for the project. The authors acknowledge the Federal University of Lafia and Muhammadu Buhari TETFund Centre of Excellence (MBTCE) for providing the required facilities for this work. Additionally, AHL appreciates Mrs. Rashidat Labulo for proofreading the draft manuscript.

References

[1] A. Baruwa, O. J. Gbadeyan & K. Permaul, "Revolutionizing biotechnology: the impact of nanocatalysts and nanomaterials—a comprehensive review", Discov. Mater. **5** (2025) 89. https://doi.org/10.1007/s43939-025-00269-9.

[2] G. N. Bosio, F. S. García Einschlag, L. Carlos & D. O. Mártire, "Recent advances in the development of novel iron–copper bimetallic photo Fenton catalysts", Catalysts **13** (2023) 159. https://doi.org/10.3390/catal13010159.

[3] Z. Świątkowska-Warkocka, "Bimetal CuFe nanoparticles—synthesis, properties, and applications", Appl. Sci. **11** (2021) 1978. https://doi.org/10.3390/app11051978.

[4] S. Devi, G. S. Sabesan & S. A. Ismail (Eds.), *Opportunities for biotechnology research and entrepreneurship*, Bentham Science Publishers, 2024. https://doi.org/10.2174/9789815196115124010l.

[5] J. Singh, T. Dutta, K.-H. Kim, M. Rawat, P. Samddar & P. Kumar, "'Green' synthesis of metals and their oxide nanoparticles: applications for environmental remediation", J. Nanobiotechnol. **16** (2018) 84. https://doi.org/10.1186/s12951-018-0408-4.

[6] D. B. Tripathy & A. Gupta, "Nanocomposites as sustainable smart materials: a review", J. Reinf. Plast. Compos. (2024). https://doi.org/10.1177/07316844241233162.

[7] A. M. E. Shafey, "Green synthesis of metal and metal oxide nanoparticles from plant leaf extracts and their applications: a review", Green Process. Synth. **9** (2020) 304. https://doi.org/10.1515/gps-2020-0031.

[8] Z. Vaseghi, A. Nematollahzadeh & O. Tavakoli, "Green methods for the synthesis of metal nanoparticles using biogenic reducing agents: a review", Rev. Chem. Eng. **34** (2018) 529. https://doi.org/10.1515/revce-2017-0005.

[9] Z. Vaseghi, O. Tavakoli & A. Nematollahzadeh, "Rapid biosynthesis of novel Cu/Cr/Ni trimetallic oxide nanoparticles with antimicrobial activity", J. Environ. Chem. Eng. **6** (2018) 1898. https://doi.org/10.1016/j.jece.2018.02.038.

[10] S. Shahzadi, S. Fatima, Q. Ul Ain, Z. Shafiq & M. R. S. A. Janjua, "A review on green synthesis of silver nanoparticles (SNPs) using plant extracts: a multifaceted approach in photocatalysis, environmental remedia-

tion, and biomedicine'', RSC Adv. **15** (2025) 3858. https://doi.org/10.1039/D4RA07519F.

[11] J. A. Aboyewa, N. R. S. Sibuyi, M. Meyer & O. O. Oguntibeju, ''Green synthesis of metallic nanoparticles using some selected medicinal plants from Southern Africa and their biological applications'', Plants **10** (2021) 1929. https://doi.org/10.3390/plants10091929.

[12] C. Rabadeaux, L. Vallette, J. Sirdaarta, C. Davis & I. E. Cock, ''An examination of the antimicrobial and anticancer properties of Khaya senegalensis (Desr.) A. Juss. bark extracts'', Pharmacogn. J. **9** (2017) 504. https://doi.org/10.5530/pj.2017.4.82.

[13] X. Xiong, C. Wu, J. J. Elser, Z. Mei & Y. Hao, ''Occurrence and fate of microplastic debris in middle and lower reaches of the Yangtze River – from inland to the sea'', Sci. Total Environ. **659** (2019) 66. https://doi.org/10.1016/j.scitotenv.2018.12.313.

[14] A. Haleem, A. Shafiq, S.-Q. Chen & M. Nazar, ''A comprehensive review on adsorption, photocatalytic and chemical degradation of dyes and nitro-compounds over different kinds of porous and composite materials'', Molecules **28** (2023) 1081. https://doi.org/10.3390/molecules28031081.

[15] R. Franco-Duarte et al., ''Advances in chemical and biological methods to identify microorganisms—from past to present'', Microorganisms **7** (2019) 130. https://doi.org/10.3390/microorganisms7050130.

[16] G. Yadav, N. Yadav & M. Ahmaruzzaman, ''Photoreduction of nitrophenol using metal oxide-based nanocomposites: a green and efficient approach for aqueous environmental remediation'', Int. J. Environ. Anal. Chem. **105** (2025) 1779. https://doi.org/10.1080/03067319.2023.2298722.

[17] K. Loza, M. Heggen & M. Epple, ''Synthesis, structure, properties, and applications of bimetallic nanoparticles of noble metals'', Adv. Funct. Mater. **30** (2020) 1909260. https://doi.org/10.1002/adfm.201909260.

[18] I. Mustieles Marín, J. M. Asensio & B. Chaudret, ''Bimetallic nanoparticles associating noble metals and first-row transition metals in catalysis'', ACS Nano **15** (2021) 3550. https://doi.org/10.1021/acsnano.0c09744.

[19] O. Elmutasim, L. M. Maghrabi, D. S. Dhawale & K. Polychronopoulou, ''Engaging the concepts of bimetallicity and mechanical strain for N_2 activation: a computational exploration'', ACS Appl. Mater. Interfaces **16** (2024) 56254. https://doi.org/10.1021/acsami.4c09691.

[20] D. S. Idris & A. Roy, ''Synthesis of bimetallic nanoparticles and applications—an updated review'', Crystals **13** (2023) 637. https://doi.org/10.3390/cryst13040637.

[21] A. Babajide, T. Adebolu, M. Oladunmoye & B. Oladejo, ''Evaluation of antibacterial activity of Citrus aurantium L. leaf extracts on bacteria isolated from blood of Hepatitis B positive individuals in Ondo State, Nigeria'', Microbes Infect. Dis. **4** (2023) 304. https://doi.org/10.21608/mid.2021.103642.1206.

[22] Y. Bibi, S. Nisa, A. Waheed, M. Zia, S. Sarwar, S. Ahmed & M. F. Chaudhary, ''Evaluation of Viburnum foetens for anticancer and antibacterial potential and phytochemical analysis'', Afr. J. Biotechnol. **9** (2010) 5611. https://doi.org/10.5555/20103289930.

[23] A. Wadood, M. Ghufran, S. B. Jamal, M. Naeem, A. Khan et al., ''Phytochemical analysis of medicinal plants occurring in local area of Mardan'', Biochem. Anal. Biochem. **2** (2013) 144. https://doi.org/10.4172/2161-1009.1000144.

[24] D. Kumar, R. Ghosh & B. C. Pal, ''α-Glucosidase inhibitory terpenoids from Potentilla fulgens and their quantitative estimation by validated HPLC method'', J. Funct. Foods **5** (2013) 1135. https://doi.org/10.1016/j.jff.2013.03.010.

[25] R. Gul, S. U. Jan, S. Faridullah, S. Sherani & N. Jahan, ''Preliminary phytochemical screening, quantitative analysis of alkaloids, and antioxidant activity of crude plant extracts from Ephedra intermedia indigenous to Balochistan'', Sci. World J. **2017** (2017) 1. https://doi.org/10.1155/2017/5873648.

[26] S. Kanagasubbulakshmi & K. Kadirvelu, ''Green synthesis of iron oxide nanoparticles using Lagenaria siceraria and evaluation of its antimicrobial activity'', Def. Life Sci. J. **2** (2017) 422. https://doi.org/10.14429/dlsj.2.12277.

[27] Z. Alhalili, ''Green synthesis of copper oxide nanoparticles CuO NPs from Eucalyptus Globoulus leaf extract: adsorption and design of experiments'', Arab. J. Chem. **15** (2022) 103739. https://doi.org/10.1016/j.arabjc.2022.103739.

[28] M. Černík & V. V. Thekkae Padil, ''Green synthesis of copper oxide nanoparticles using gum karaya as a biotemplate and their antibacterial application'', Int. J. Nanomedicine **2013** (2013) 889. https://doi.org/10.2147/IJN.S40599.

[29] O. A. Fabiyi, A. H. Labulo, A. V. Ogundele, T. A. Adesalu, H. S. Mella, O. B. Akinsipo & A. O. Claudius-Cole, ''Assessment and nematicidal activity of Cu/Fe and Zn/Fe bimetallic nanoparticles against root-knot nematode in beetroot and cabbage'', Sci. Rep. **15** (2025) 29165. https://doi.org/10.1038/s41598-025-14384-3.

[30] M. Yoro, J. D. Samson, J. Joshua, J. W. K. Jonah, P. D. Bello, D. G. Ajima & N. Umar, ''Biosynthesis, optimization of process parameters and antimicrobial activity of silver nanoparticles from Moringa oleifera leaf extract'', Compr. Res. Rev. Chem. Pharm. **1** (2022) 001. https://doi.org/10.57219/crrcp.2022.1.1.0001.

[31] B. I. Iotsor, F. Iseghohi, O. E. Oladoja, O. R. Raji, Z. Yusuf & O. A. Oyewole, ''Antimicrobial activities of garlic and ginger extracts on some clinical isolates'', Int. J. Biotechnol. **8** (2019) 59. https://doi.org/10.18488/journal.57.2019.81.59.65.

[32] A. M. Bobenchik, J. A. Hindler, C. L. Giltner, S. Saeki & R. M. Humphries, ''Performance of Vitek 2 for antimicrobial susceptibility testing of Staphylococcus spp. and Enterococcus spp'', J. Clin. Microbiol. **52** (2014) 392. https://doi.org/10.1128/JCM.02432-13.

[33] U. Kosikowska et al., ''Prevalence of susceptibility patterns of opportunistic bacteria in line with CLSI or EUCAST among Haemophilus parainfluenzae isolated from respiratory microbiota'', Sci. Rep. **10** (2020) 11512. https://doi.org/10.1038/s41598-020-68161-5.

[34] A. U. Khan et al., ''A facile fabrication of silver/copper oxide nanocomposite: an innovative entry in photocatalytic and biomedical materials'', Photodiagn. Photodyn. Ther. **31** (2020) 101814. https://doi.org/10.1016/j.pdpdt.2020.101814.

[35] S. K. Maji, N. Mukherjee, A. Mondal & B. Adhikary, ''Synthesis, characterization and photocatalytic activity of α-Fe_2O_3 nanoparticles'', Polyhedron **33** (2012) 145. https://doi.org/10.1016/j.poly.2011.11.017.

[36] B. Y. Yu & S.-Y. Kwak, ''Carbon quantum dots embedded with mesoporous hematite nanospheres as efficient visible light-active photocatalysts'', J. Mater. Chem. **22** (2012) 8345. https://doi.org/10.1039/c2jm16931b.

[37] M. Fazlzadeh, K. Rahmani, A. Zarei, H. Abdoallahzadeh, F. Nasiri & R. Khosravi, ''A novel green synthesis of zero valent iron nanoparticles (NZVI) using three plant extracts and their efficient application for removal of Cr(VI) from aqueous solutions'', Adv. Powder Technol. **28** (2017) 122. https://doi.org/10.1016/j.apt.2016.09.003.

[38] L. Qian & B. Chen, ''Interactions of aluminum with biochars and oxidized biochars: implications for the biochar aging process'', J. Agric. Food Chem. **62** (2014) 373. https://doi.org/10.1021/jf404624h.

[39] J. Liu, Q. Zhang, F. Ma, S. Zhang, Q. Zhou & A. Huang, ''Three-step identification of infrared spectra of similar tree species to Pterocarpus santalinus covered with beeswax'', J. Mol. Struct. **1218** (2020) 128484. https://doi.org/10.1016/j.molstruc.2020.128484.

[40] S. Pasieczna-Patkowska, M. Cichy & J. Flieger, ''Application of Fourier transform infrared (FTIR) spectroscopy in characterization of green synthesized nanoparticles'', Molecules **30** (2025) 684. https://doi.org/10.3390/molecules30030684.

[41] R. D. Neal, Y. Inoue, R. A. Hughes & S. Neretina, ''Catalytic reduction of 4-nitrophenol by gold catalysts: the influence of borohydride concentration on the induction time'', J. Phys. Chem. C **123** (2019) 12894. https://doi.org/10.1021/acs.jpcc.9b02396.

[42] S. Guo, M. B. Isah, R. Hu, Z. Guo, X. Wei, Z. Liu & X. Zhang, ''A metal-based heterojunction for controlled release of multiple cations and reactive oxygen species inhibiting multidrug-resistant bacteria in vitro and in vivo'', ACS Appl. Mater. Interfaces **17** (2025) 38859. https://doi.org/10.1021/acsami.5c05798.

[43] A. B. Lorusso, J. A. Carrara, C. D. N. Barroso, F. F. Tuon & H. Faoro, ''Role of efflux pumps on antimicrobial resistance in Pseudomonas aeruginosa'', Int. J. Mol. Sci. **23** (2022) 15779. https://doi.org/10.3390/ijms232415779.

[44] O. Antonoglou, K. Lafazanis, S. Mourdikoudis, G. Vourlias, T. Lialiaris, A. Pantazaki & C. Dendrinou-Samara, ''Biological relevance of $CuFeO_2$ nanoparticles: antibacterial and anti-inflammatory activity, genotoxicity, DNA and protein interactions'', Mater. Sci. Eng. C **99** (2019) 264. https://doi.org/10.1016/j.msec.2019.01.112.

[45] E. Arulkumar, R. K. Manivannan, G. Dhamodaran & R. Krishnan, ''CuO@α-Fe_2O_3 nanocomposite via one-pot synthesis for multifunctional photocatalytic, optoelectronic and antimicrobial applications'', J. Sol-Gel Sci. Technol. **116** (2025) 2505. https://doi.org/10.1007/s10971-025-06851-0.

[46] O. Ciofu & T. Tolker-Nielsen, ''Tolerance and resistance of Pseudomonas aeruginosa biofilms to antimicrobial agents—how P. aeruginosa can escape antibiotics'', Front. Microbiol. **10** (2019) 913. https://doi.org/10.3389/fmicb.2019.00913.

[47] A. Anurag Anand, A. Amod, S. Anwar, A. K. Sahoo, G. Sethi & S. K. Samanta, ‘‘A comprehensive guide on screening and selection of a suitable AMP against biofilm-forming bacteria’’, Crit. Rev. Microbiol. **50** (2024) 859. https://doi.org/10.1080/1040841X.2023.2293019.

[48] S. O. Ogunyemi, Y. Abdallah, E. Ibrahim, Y. Zhang, J. A. Bi, F. Wang & L. Xu, ‘‘Bacteriophage-mediated biosynthesis of MnO_2NPs and MgONPs and their role in the protection of plants from bacterial pathogens’’, Front. Microbiol. **14** (2023) 1193206. https://doi.org/10.3389/fmicb.2023.1193206.